Arch Toxicol (2016) 90:2231–2248
DOI 10.1007/s00204-016-1711-1

IMMUNOTOXICOLOGY

In vivo activation of a T helper 2-driven innate immune response in lung fibrosis induced by multi-walled carbon nanotubes

Jie Dong[1] · **Qiang Ma**[1]

Received: 3 February 2016 / Accepted: 11 April 2016 / Published online: 22 April 2016

Abstract Pulmonary exposure to certain forms of carbon nanotubes (CNT) induces fibrosing lesions in the lungs that manifest an acute inflammation followed by chronic interstitial fibrosis. The mechanism of CNT-induced fibrogenesis is largely unknown. The biphasic development with drastically distinct pathologic manifestations suggests a junction of acute-to-chronic transition. Here we analyzed the molecular pathways and regulators underlying the pathologic development of CNT-induced lung fibrosis. Mice were exposed to multi-walled CNT (MWCNT; XNRI MWNT-7, Mitsui; 40 μg) by pharyngeal aspiration for 7 days along with vehicle and carbonaceous controls. Genome-wide microarray analyses of the lungs identified a range of differentially expressed genes that potentially function in the acute-to-chronic transition through pathways involving immune and inflammatory regulation, responses to stress and extracellular stimuli, and cell migration and adhesion. In particular, a T helper 2 (Th2)-driven innate immune response was significantly enriched. We then demonstrated that MWCNT induced the expression of Th2 cytokines interleukin (IL)-4 and IL-13, and a panel of signature downstream genes, such as Il4i1, Chia, and Ccl11/Eotaxin, time dependently. Induction of Th2 cytokines took place in CD4+ T lymphocytes indicating activation of Th2 cells. Furthermore, induction involved activation of a Th2 cell-specific signaling pathway through phosphorylation of STAT6 and up-regulation of GATA-3 to mediate the transcription of Th2 target genes. Our study uncovers activation of a Th2-driven immune/inflammatory response during pulmonary fibrosis development induced by MWCNT. The findings provide novel insights into the molecular events that control the transition from an acute inflammatory response to chronic fibrosis through Th2 functions in CNT-exposed lungs.

Keywords Multi-walled carbon nanotubes · Th2-type response · Pulmonary fibrosis · IL-4 · IL-13

Abbreviations

BAL	Bronchoalveolar lavage
Ccl11	Chemokine (C–C motif) ligand 11, or eotaxin
Chia	Chitinase, acidic, or AMCase
CNT	Carbon nanotubes
DM	Dispersion medium
ELISA	Enzyme-linked immunosorbent assay
FDR	False discovery rate
FN1	Fibronectin
GAPDH	Glyceraldehyde 3-phosphate dehydrogenase
GATA-3	GATA-binding protein 3
GO	Gene ontology
IL	Interleukin
Il4i1	Interleukin 4 induced 1, or Fig. 1
IL-4Rα	IL-4 receptor α
MWCNT	Multi-walled carbon nanotubes
STAT6	Signal transducer and activator of transcription 6

The findings and conclusions in this report are those of the authors and do not necessarily represent the views of the National Institute for Occupational Safety and Health.

Electronic supplementary material The online version of this article (doi:10.1007/s00204-016-1711-1) contains supplementary material, which is available to authorized users.

✉ Qiang Ma
qam1@cdc.gov

[1] Receptor Biology Laboratory, Toxicology and Molecular Biology Branch, Health Effects Laboratory Division, National Institute for Occupational Safety and Health, Centers for Disease Control and Prevention, Mailstop 3014, 1095 Willowdale Road, Morgantown, WV 26505, USA

SWCNT	Single-walled carbon nanotubes
Th0	Naïve T helper
Th1	T helper 1
Th2	T helper 2
TSLP	Thymic stromal lymphopoietin

Introduction

Fibrosis is a final, common pathological outcome of many chronic inflammatory diseases that frequently leads to organ failure with high rates of mortality and disability (Duffield et al. 2013; Wynn and Ramalingam 2012). The mechanism(s) underlying pathologic fibrosis development is poorly understood despite decades of intensive research. The lungs are among the most susceptible organs to fibrosis, which is in part due to their function as the site of gas exchange between the blood and inhaled air through a thin layer of alveolar septal structures (Husain and Kumar 2005; Morgan and Seaton 1995). Moreover, the lungs are constantly exposed to numerous fibrosis-inducing agents, such as particles and fibers, from inhaled air. An improved fundamental understanding of the molecular mechanism(s) governing fibrogenesis is much needed for developing effective prevention and therapy against deadly fibrosing diseases.

Carbon nanotubes (CNT) are new nanomaterials with a variety of industrial and commercial applications ranging from electronic inventions to biomedical uses (De Volder et al. 2013; Zhang et al. 2013). CNT are respirable and tend to accumulate in the lungs owing to their fiber-like shape and high biopersistence, attributes known to cause the fibrogenic and carcinogenic effects of inhaled particles and fibers (Dong and Ma 2015a). In animal studies, CNT behave as inflammogenic and fibrogenic agents in the lung parenchyma and pleural space in size, shape, and surface property-dependent manners (Donaldson et al. 2010; Dong and Ma 2015a; Johnston et al. 2010). The possibility that exposure to CNT can lead to lung fibrosing disease in humans has received a particular attention in occupational, environmental, and consumer product safety evaluation of nanoexposure. Assessment of nanosafety is requisite, but

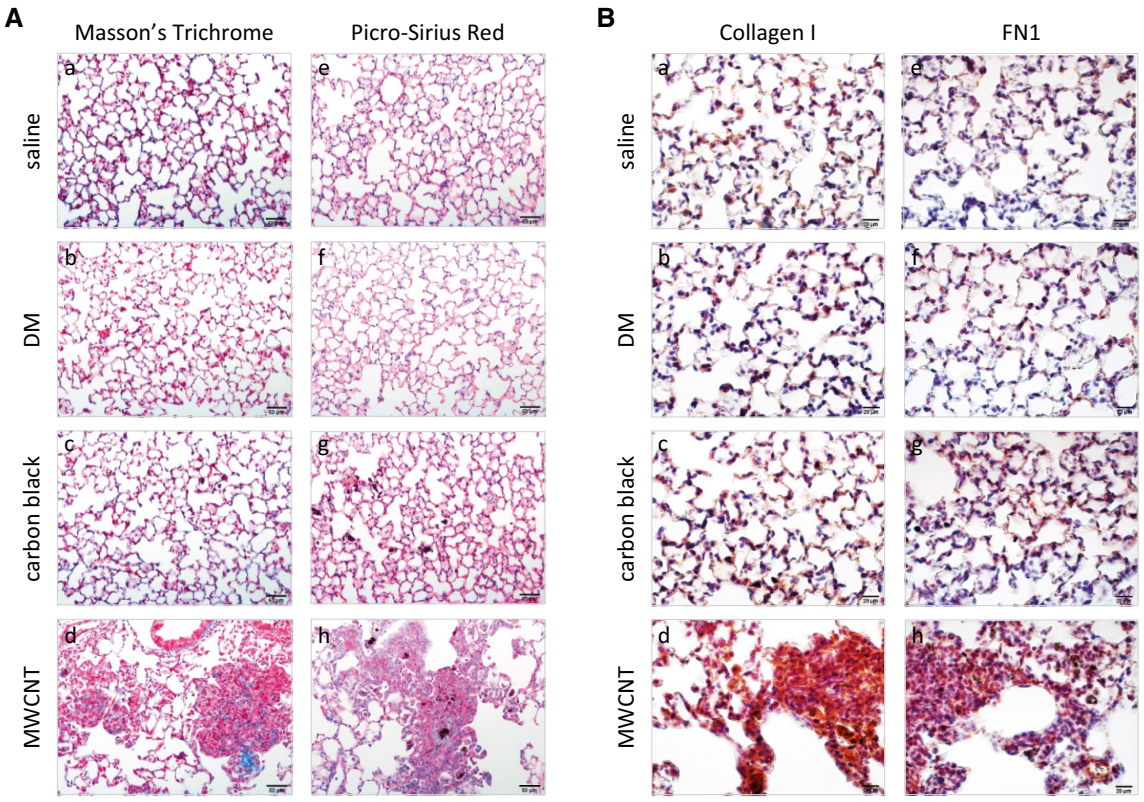

Fig. 1 Lung fibrosis induced by MWCNT. Wild-type C57BL/6J mice received saline, DM vehicle, carbon black (40 μg per mouse) or MWCNT (40 μg per mouse) and were killed on day 7 post-exposure. **A** Total collagen fibers were detected by Masson's Trichrome staining of lung tissue sections, with collagen fibers stained blue (*a–d scale bar* 50 μm). Collagen I and III fibers were visualized by Picro-Sirius Red staining, with collagen fibers stained red (*e–h scale bar* 50 μm). **B** Collagen I (*a–d*) and FN1 (*e–h*) protein expression was determined by immunohistochemistry on lung sections. *Red* indicates positive staining, and *blue* indicates nuclear counterstaining (*scale bar* 20 μm)

has been hindered by a paucity of mechanistic insights into the pulmonary effect of nanoexposure (Dong and Ma 2015a).

The lung lesions elicited by CNT, either multi-walled (MWCNT) or single-walled (SWCNT), resemble the pulmonary response to deposition of foreign bodies such as insoluble dusts (i.e., silica, asbestos, and coal dust) and large biologic masses (i.e., inhaled allergens and microbes, and invading parasites), all of which are capable of inducing lung fibrosis (Dong and Ma 2015a; Dong et al. 2015a, b; Husain and Kumar 2005; Morgan and Seaton 1995). The response initiates with a prominent acute inflammation, indicated by recruitment and accumulation of inflammatory cells and elevated secretion of cytokines and growth factors. In the case of persistent deposition, chronic progression to fibrosis would ensue, resulting in fibrous extracellular matrix deposition, thickened alveolar septa, enhanced expression of fibrosis marker proteins, and formation of fibrotic foci and epithelioid granulomas in lung tissues (Aiso et al. 2010; Dong et al. 2015a; Porter et al. 2010; Reddy et al. 2012; Wang et al. 2013). We recently demonstrated that MWCNT trigger a rapid-onset fibrotic response, detectable as early as day 1 post-exposure and at a dose as low as 5 μg per mouse, revealing that MWCNT confer a potent fibrogenic effect that takes place alongside the acute inflammatory response upon exposure and is converted into chronic pathologic fibrosis in the lungs after 2 weeks of exposure (Dong et al. 2015a). The biphasic nature of the lesions and the drastically distinct pathologic phenotypes between the two phases suggest a critical transition between the acute and chronic phase responses that promotes the pathologic progression from acute inflammation to chronic fibrosis.

In this study, we attempted to dissect the mechanism(s) by which CNT induce lung fibrosis. Genome-wide gene expression microarray analysis was performed to target on altered gene expression during the acute-to-chronic transition in mouse lungs exposed to MWCNT. Dysregulated gene expression, signaling pathways, cellular functions, and transcription networks in response to MWCNT exposure were identified. Importantly, multiple assays consistently identified a T helper 2 (Th2)-driven response to be significantly activated by MWCNT in mouse lungs. Given the implicated manifold roles of Th2 response in fibrosis development, we examined in depth the activation of Th2 response in CNT-induced lung fibrotic lesions. The findings reveal that Th2 cytokines IL-4 and IL-13 were significantly induced in the lungs and a subset of CD4+ T cells displayed enhanced expression of IL-4 and IL-13, indicating the differentiation and activation of Th2 lymphocytes. The transcription factor STAT6 (signal transducer and activator of transcription 6) was activated through phosphorylation of the protein, and GATA-3 (GATA-binding protein 3) expression was up-regulated, leading to increased transcription of Th2 cytokines. Our study uncovers that exposure to MWCNT triggers Th2-type cytokine expression and secretion, Th2 cell differentiation, and Th2 cell-specific signaling in the lungs, which strongly supports activation of a Th2-driven innate immune response as a novel mechanism to initiate and boost MWCNT-induced lung fibrosis.

Materials and methods

Animals and MWCNT

Eight- to 10-week-old male C57BL/6J mice purchased from The Jackson Laboratory (Bar Harbor, ME, USA) were used. Mice were maintained in an accredited, specific pathogen-free, and environmentally controlled facility at the National Institute for Occupational Safety and Health (NIOSH). Mice were housed in polycarbonate ventilated cages with 12-h fluorescent lighting and fed with Harlan Teklad Rodent Diet 7913 (Indianapolis, IN, USA) with tap water ad libitum. Autoclaved Alpha-Dri virgin cellulose chips and hardwood beta-chips were used as bedding. All animal studies were approved by IACUC (Institutional animal care and use committee).

The MWCNT used in this study were obtained from Mitsui and Company (XNRI MWNT-7, lot #05072001K28). This lot was fully characterized in previous reports, in which acute and subchronic exposures were conducted (Dong et al. 2015a; Porter et al. 2010). The MWCNT have an average surface area of 26 m^2/g as measured by nitrogen absorption–desorption technique (Brunauer-Emmett-Teller method, or BET); and a median length of 3.86 μm and count mean diameter of 49 ± 13.4 nm, as determined by scanning electron microscopy when suspended in a dispersion medium (DM). Trace element contaminations were low, with 0.78 % for all metals, 0.41 % for sodium, and 0.32 % for iron. DM containing Ca^{2+}- and Mg^{2+}-free phosphate buffered saline (PBS), pH7.4, 0.6 mg/ml mouse serum albumin (Sigma, St. Louis, MO, USA) and 0.01 mg/ml 1,2-dipalmitoyl-sn-glycerol-3-phosphocholine (Sigma) was used to suspend carbon black and MWCNT. DM was prepared and MWCNT were effectively dispersed in DM with sonication immediately before use; the preparation does not cause toxicity or mask surface activity of MWCNT at the dose used in this study (see "Results" section).

Animal treatment

Mice were dosed with (a) saline (Baxter Healthcare Corporation, Deerfield, IL, USA), 50 μl/mouse; (b) freshly prepared DM, 50 μl/mouse; (c) carbon black (Degussa

Engineered Carbons LP, Parsippany, NJ, USA), 40 μg/mouse in 50 μl DM; or (d) MWCNT, 40 μg/mouse in 50 μl DM, by pharyngeal aspiration. The dose of MWCNT used was based on previous dose–response studies, in which pulmonary exposure to MWCNT at 40 μg induced apparent acute inflammation and chronic fibrosis in mouse lungs (Dong et al. 2015a; Porter et al. 2010). Pharyngeal aspiration was performed following established procedures. This alternative to inhalation produces an even distribution of particles throughout the lungs, thus representing a physiologically relevant and noninvasive route of administration to deliver a specific dose into mouse lungs. Mice were monitored for general health and toxicity daily after treatment. Mouse body weights were recorded, and there were no significant differences in the initial body weights among exposed groups. No apparent effect from treatment on the overall health status was observed during experiment.

Histopathology

Mice were euthanized by intraperitoneal injection of sodium pentobarbital at a dose of >100 mg/kg body weight (Zoetis, Florham Park, NJ, USA). The left lung lobe was removed, fixed with 10 % neutral buffered formalin through intratracheal perfusion, and embedded in paraffin. Sections of 5 μm thickness were subjected to Masson's Trichrome staining and Picro-Sirius Red staining following standard protocols.

Microarray gene expression analysis

Total RNA was extracted from mouse lung tissue samples using RNeasy Mini Kit (QIAGEN, Valencia, CA, USA), during which genomic DNA was removed with the method of on-column DNase treatment. RNA samples from four mice in each treated group were selected randomly and were used for microarray analysis. All the RNA samples used for this assay reached the required quality, including (a) an A260/A280 ratio between 1.8 and 2.1; (b) an A260/A230 ratio greater than 1.5; and (c) an RNA Integrity Score (RIN score) of 8 or greater evaluated by an Agilent 2100 Bioanalyzer (Agilent Technologies, Santa Clara, CA, USA).

The cRNA was synthesized from total RNA using Illumina TotalPrep RNA Amplification Kit (Life Technologies, Carlsbad, CA, USA) and hybridized to MouseWG-6 v2.0 Expression BeadChip (Illumina, San Diego, CA, USA). The raw data were processed with Illumina HiScan Array Scanner and GenomeStudio software v1.9.0 (Illumina), through microarray services at Yale Center for Genome Analysis (Yale University School of Medicine, New Haven, CT, USA).

Microarray data analyses were carried out under a service at Yale Bioinformatics Resources (Yale University School of Medicine). Briefly, gene expression data generated by Illumina were imported into Partek® Genomics Suite™ (Partek Incorporated, 6.4), and raw data were processed in steps of background correction of the perfect match values, quintile normalization across all of the chips in the experiment, and median polish summarization. Under each condition, outliers were identified using principle component analysis (PCA) and were excluded from all further analysis. Differential expression analysis of the samples was performed using one-way analysis of variance (ANOVA). p values were adjusted for multiple comparisons using FDR (false discovery rate) multiple testing correction. Differentially expressed genes in the MWCNT-treated group, compared with the DM-treated group, were selected with a threshold of relative ±1.5-fold change and with p value with FDR ≤ 0.05. The heat map was generated using heatmap.2 function available in "gplots" package in R program.

Enriched canonical pathways, process networks, and gene ontology (GO) cellular processes associated with identified differentially expressed genes were disclosed using MeteCore GeneGO server (https://portal.genego.com/). p values were calculated based on hypergeometric distribution and reflected the probability for a pathway or process to arise by chance. Pathways and processes with a Benjamini–Hochberg Multiple Testing Correction p value of ≤ 0.05 were considered significant. The network-building algorithm on transcription regulation from MetaCore was used to examine whether the identified genes were connected to transcription factors. For each candidate transcription factor, a p value was calculated based on hypergeometric distribution, indicating enrichment in the genes of interest. Transcription factors with Benjamini–Hochberg Multiple Testing Correction p value of ≤ 0.05 were considered significant. Transcription regulation networks were built centering on the most significant transcription factors.

Quantitative RT-PCR (qRT-PCR)

Total RNA was extracted from mouse lungs using RNeasy Mini Kit. One μg of total RNA was reversely transcribed in a 20 μl reaction with QuantiTect Reverse Transcription system (Qiagen) to produce cDNA, which was then diluted at 1:10 with nuclease-free water, and 5 μl of diluted cDNA products was used as template for PCR analysis. Real-time PCR was performed using RT^2 SYBR Green ROX qPCR Mastermix (Qiagen) with ABI Sequence Detection System 7500 (Life Technologies). Mouse housekeeping gene glyceraldehyde 3-phosphate dehydrogenase (*Gapdh*) was used as an internal control

for normalization in all PCRs. Primer sequences are available upon request. Fold change for each gene was calculated as previously described (Dong et al. 2015a). The fold change values for three samples in each experimental group were averaged, and data were presented as the mean ± standard deviation (SD).

Lung homogenization and cytokine measurement

Right lung lobes were removed and homogenized in 0.5 ml of T-PER Tissue Protein Extraction Reagent (Life Technologies) containing Complete Protease Inhibitor Cocktail Tablets (Roche, Basel, Switzerland) to obtain lung tissue extract. The extract was centrifuged at 10,000×*g* for 5 min at 4 °C to remove cell debris, and the supernatant was used to perform enzyme-linked immunosorbent assay (ELISA) for the protein level of CCL11/Eotaxin, with Mouse DuoSet ELISA assay kit (R&D Systems, Minneapolis, MN, USA). An optical density at 450 nm was obtained using SPECTRA max 384 PLUS (Molecular Devices, Sunnyvale, CA, USA). Samples from four animals per treatment group were measured and calculated as mean ± SD.

Immunohistochemistry

Formalin-fixed, paraffin-embedded lung tissue sections (left lung lobe, 5 μm) were deparaffinized, antigen-unmasked, and endogenous peroxidase and alkaline phosphatase-blocked, as previously described (Dong et al. 2015a). The assays were performed with ImmPRESS Polymer Detection system (Vector Laboratories, Burlingame, CA, USA), following instructions from the manufacturer. When mouse primary antibody was applied, the blocking reagent and antibody diluent from the M.O.M. Immunodetection Kit (Vector Laboratories) were used to eliminate background staining. Peroxidase activities were detected with the peroxidase substrate ImmPACT NovaRED (Vector Laboratories), which generates positive staining with red color; and the slides were counterstained with Hematoxylin QS (Vector Laboratories), which visualizes nuclei with blue-violet color. The primary antibodies used for immunohistochemistry included anti-Collagen I (Abcam, Cambridge, MA, USA), anti-FN1 (Abcam), anti-IL-4 (Thermo Fisher Scientific, Rockford, IL, USA), anti-IL-13 (GeneTex, Irvine, CA, USA), anti-p-STAT6 (phospho Y641, Abcam, ab28829), anti-GATA-3 (Santa Cruz Biotechnology, Dallas, Texas, USA), anti-IL4I1 (Biorbyt, San Francisco, CA, USA), anti-CHIA (Abcam), and anti-CCL11/Eotaxin (Bioss Antibodies, Woburn, MA, USA). Images were photographed using Olympus Provis AX-70 system (Olympus, Center Valley, PA, USA). Quantification of positive staining was carried out using the ImageJ program (National Institutes of Health, Bethesda, MA, USA); and the levels of relative intensity were compared and presented ($n = 4$).

Immunofluorescence

Cryostat sections from frozen lung tissues (left lung lobe, 7 μm) were prepared and fixed with 4 % paraformaldehyde at room temperature for 10 min. After being blocked for 1 h at room temperature, slides were immunostained with primary antibodies at 4 °C overnight, incubated with Alexa Fluor 488- or Alexa Fluor 594-conjugated secondary antibodies (Life Technologies) for 1 h at room temperature in dark, and mounted with ProLong Gold Antifade Mountant with DAPI (Life Technologies). When mouse primary antibody was applied, the blocking reagent and antibody diluent from the M.O.M. Immunodetection Kit were used to eliminate background staining. The primary antibodies used for immunofluorescence were Alexa Fluor 594 anti-mouse CD4 (BioLegend, San Diego, CA, USA), anti-CD45R/B220 (eBioscience, San Diego, CA, USA), and the antibodies detecting IL-4, IL-13, p-STAT6 and GATA-3 used in immunohistochemistry (described above). Images were taken with a Zeiss LSM 510 confocal microscope (Carl Zeiss Microscopy, Jena, Germany).

Immunoblotting

Lung tissue samples were homogenized in CelLytic MT Cell Lysis Reagent (Sigma) containing Complete Protease Inhibitor Cocktail Tablets, followed by incubation on ice for 30 min with shaking, and centrifugation at 14,000 rpm for 20 min at 4 °C to remove cell debris. The supernatant containing the whole protein extract was obtained, of which 20 μg was resolved in 4–15 % Criterion Tris–HCl Gel (Bio-Rad, Hercules, CA, USA), transferred to PVDF membrane (EMD Millipore, Billerica, MA, USA), blocked with SuperBlock T20 (PBS) Blocking Buffer (Thermo Fisher Scientific) at room temperature for 1 h, incubated with primary antibodies at 4 °C overnight, incubated with horseradish peroxidase-conjugated secondary antibodies at room temperature for 1 h, and detected using Amersham ECL Prime Western Blotting Detection Reagent (GE Healthcare Life Sciences, Little Chalfont, Buckinghamshire, UK). GAPDH was detected as a loading control. The primary antibodies used for immunoblotting were anti-p-STAT6 (phospho Y641, Abcam, ab54461), anti-STAT6 (Cell Signaling Technology, Danvers, MA, USA), anti-GAPDH (Fitzgerald, Acton, MA, USA), and the antibodies detecting GATA-3, IL4I1 and CHIA used in immunohistochemistry (described above).

Statistical analysis

Statistical evaluation of differences between experimental groups was determined by one-way ANOVA using the online one-way ANOVA with post hoc Tukey HSD Test Calculator at http://statistica.mooo.com. All quantitative experiments were repeated at least once with consistent results. Data were presented as Mean ± SD. A p value of less than 0.05 was considered statistically significant ($*p < 0.05$; $**p < 0.01$; and $***p < 0.001$).

Results

Pulmonary inflammation and fibrosis induced by MWCNT at the junction of acute-to-chronic transition

We have previously reported that the pulmonary lesion leading to fibrosis induced by MWCNT includes an acute phase response followed by a chronic phase progression (Dong et al. 2015a). This remarkable pathologic switch from acute-to-chronic phase response suggests there occur significant changes in the biologic functions and pathways that potentially govern fibrosis development during the acute-to-chronic transition. Presumably, this transition involves programmatic activation of gene transcription. Therefore, we attempted to analyze the gene expression profile induced by MWCNT on day 7 post-exposure, which would represent a junction of acute-to-chronic transition.

We first characterized the fibrotic and inflammatory phenotypes of mouse lungs on day 7 post-exposure to a single dose of MWCNT (40 μg, pharyngeal aspiration), which would produce both acute and chronic lesions (Dong et al. 2015a; Porter et al. 2010). Saline was used to establish a baseline lung morphology and pathology. Carbon black is a carbon-based, non-fiber shaped material with a similar chemical composition to that of CNT and thus serves as an amorphous, carbonaceous control for fiber-like shaped MWCNT. DM was used as the vehicle control for both MWCNT and carbon black.

Exposure to DM or carbon black (40 μg/mouse) for 7 days did not induce significant histopathological alterations in the lungs compared with saline control; the lung morphology appeared normal with intact alveolar structures and little inflammatory or fibrotic changes were detected by Masson's Trichrome or Picro-Sirius Red staining (Fig. 1A, a–c, e–g). These observations were consistent with previous reports that DM does not cause apparent pulmonary lesions (Porter et al. 2010), and carbon black behaves as an inactive, low-toxicity dust that does not cause significant lung inflammation and fibrosis at the dose employed in this study (Lam et al. 2004; Ma-Hock et al. 2013; Shvedova et al. 2005). In contrast, remarkable fibrotic phenotypes were observed in the lungs exposed to MWCNT (40 μg), indicated by significantly elevated deposition of collagen fibers and formation of inflammatory and fibrotic foci, which were most apparent near MWCNT deposits (Fig. 1A, d, h). Infiltration of macrophages was evident, whereas that of neutrophils was minimal, indicating a partial resolution of the early phase acute inflammation by day 7 post-exposure to MWCNT.

The specificity of MWCNT-induced fibrotic pathology was further characterized by analyzing the tissue expression and deposition of Collagen I and fibronectin (FN1), two major components of extracellular matrix proteins and markers of fibrosis. The levels of both proteins were dramatically elevated in the lungs exposed to MWCNT (Fig. 1B, d, h), but not to DM or carbon black (Fig. 1B, b and f, c and g), compared with saline control (Fig. 1B, a, e). Therefore, MWCNT, but not DM vehicle or carbon black, induced a lung fibrotic response and pathological phenotypes on day 7 post-exposure, which represents a transition from the acute response to chronic progression in CNT-induced lung fibrosis.

Microarray analysis of gene expression induced by MWCNT

To perform genome-wide microarray analysis, RNA samples from lungs of four randomly selected mice exposed to MWCNT for 7 days were analyzed individually, compared with saline, DM, or carbon black control. Differentially expressed genes induced by MWCNT were identified where a p value with the false discovery rate (FDR) was ≤ 0.05, and the fold change, either up-regulated or down-regulated, was more than 1.5, compared with DM control.

Microarray analysis revealed that among the three control groups, i.e., saline, DM, and carbon black, mild changes in gene expression in both the numbers of genes affected and the levels of changes were observed, which are a remarkable contrast to the drastically elevated or reduced expression of many genes observed in MWCNT-treated group (Fig. 2A, Table S1). Therefore, the effect of saline, DM or carbon black on gene expression relating to lung fibrosis is considered minimal in the testing system, which is consistent with the pathologic observation that there was a lack of significant morphologic alterations in saline, DM or carbon black-exposed lungs (Fig. 1). Within the controls, some DM-exposed lungs showed mild but measurable alterations of expression of certain genes compared with saline control, and certain individual variability was observed within the groups (Fig. 2A). Variations of this magnitude in control groups can be expected from a

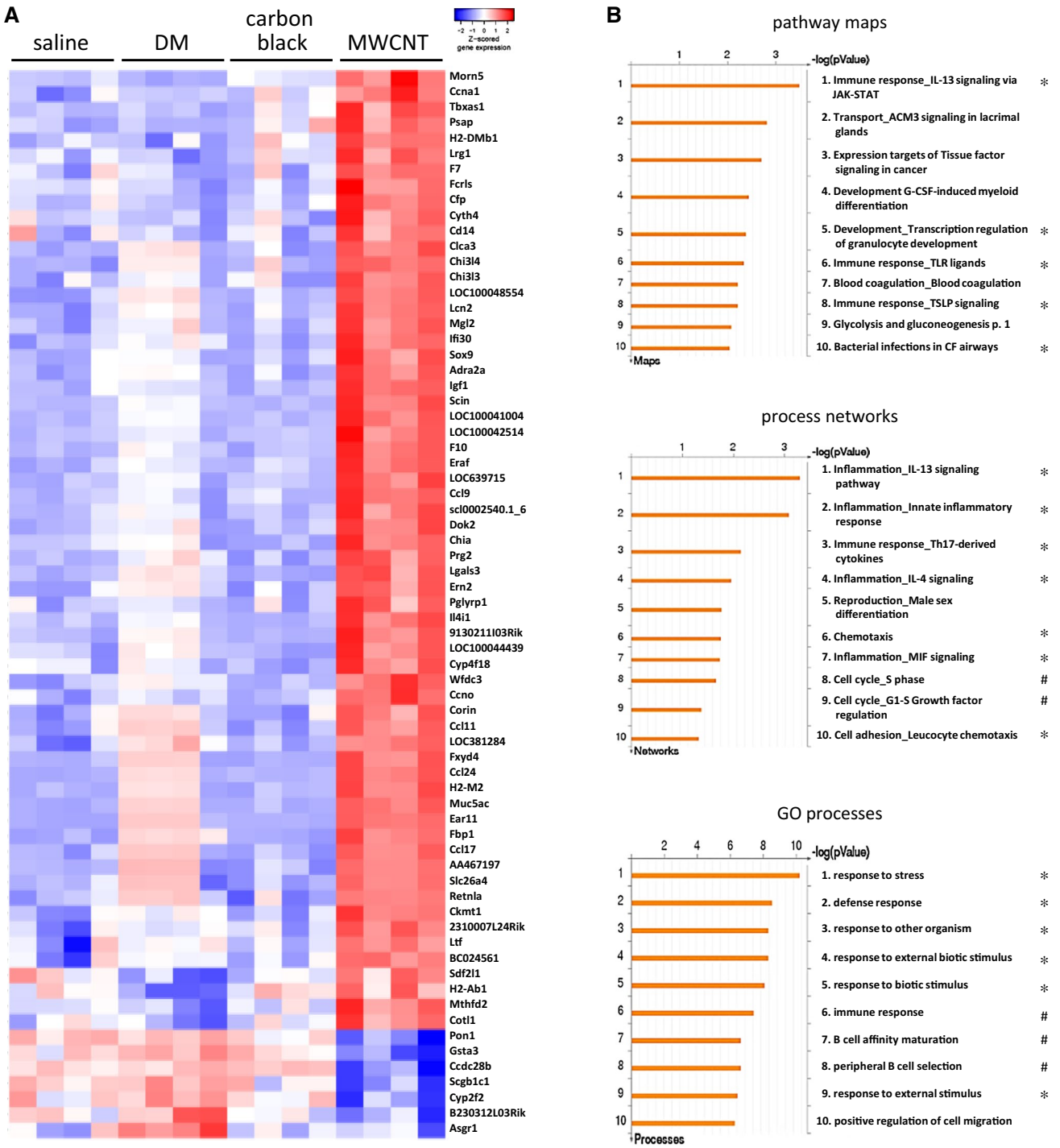

Fig. 2 Microarray analyses. Genome-wide gene expression profiling was obtained on RNA samples isolated from lungs exposed to saline, DM, carbon black (40 μg per mouse), or MWCNT (40 μg per mouse) for 7 days ($n = 4$ for each group). **A** A heat map was generated for differentially expressed genes. *Red*, *white* and *blue* indicate high, medium and low expression levels, respectively. **B** Top 10 statistically significant canonical pathways (*upper panel*), cellular processes (*middle panel*), and GO-identified cellular functions (*lower panel*) enriched by MWCNT were presented

randomly designed experimental analysis and were dealt with by using group comparisons between MWCNT- and DM-treated groups.

Compared with DM vehicle, treatment with MWCNT caused significant alterations in the expression of 69 genes, among which 62 genes were up-regulated and 7 genes

down-regulated, and the magnitudes of alterations were apparently large (Fig. 2A, Table S1). These findings indicate that the microarray analysis identified differential gene expression specific to MWCNT exposure.

Canonical pathway, functional process, gene ontology (GO), and transcriptional network activated in MWCNT-exposed lungs

We performed computational analyses of the differentially expressed genes displayed in the heat map (Fig. 2A). Canonical pathways enriched by MWCNT were identified, and top 10 statistically significant pathways were presented (Fig. 2B, top panel). Remarkably, five of the 10 pathways are related to immune and inflammatory responses (indicated by *) including IL-13 signaling via JAK-STAT, transcription regulation of granulocyte development, TLR (Toll-like receptor) ligands, TSLP (thymic stromal lymphopoietin) signaling, and bacterial infections in CF airways.

The cellular and molecular processes activated by MWCNT were analyzed, and top 10 statistically significant processes are shown in Fig. 2B (middle panel). Among the top 10 processes, seven are related to immune and inflammatory responses (indicated by *) including the IL-13 signaling pathway, innate inflammatory response, Th17-derived cytokines, IL-4 signaling, chemotaxis, MIF signaling, and cell adhesion in leukocyte chemotaxis. Thus, both the canonical pathway and the biological process analyses identified immune and inflammatory responses as a major manifestation of gene expression altered by MWCNT. In particular, activation of IL-13/IL-4 signaling central to the activation of Th2-type immune responses was identified as the most dominant function activated from both analyses; and TSLP signaling important for the initiation of Th2 responses was shown to be activated by MWCNT from canonical pathway analysis. These findings suggest that a Th2-type immune/inflammatory response(s) was preferentially induced by MWCNT in the lungs. Additionally, two processes relating to cell cycle regulation were revealed (Fig. 2B, middle panel, indicated by #). This finding is consistent with previous reports that exposure to MWCNT caused a G1/S block in cultured cells (Han et al. 2012; Siegrist et al. 2014).

Gene ontology (GO) enrichment analysis was performed to identify cellular functions involved. Top 10 statistically significant GO functions are presented in Fig. 2B (bottom panel). Six of the 10 GO processes activated by MWCNT involve responses to and defense against stress and extracellular stimuli, such as biotic stimuli, organisms, and foreign bodies (indicated by *), reflecting that MWCNT likely behave as a foreign body when deposited in the lungs. Three GO processes representing immune functions were enriched (indicated by #), further emphasizing a prominent immune involvement in MWCNT-induced pulmonary lesions. Regulation of cell migration was also identified by GO analysis.

We then analyzed the upstream regulators, transcription factors, and signaling networks that potentially mediate differential gene expression induced by MWCNT exposure. Functional analyses of both up-regulated and down-regulated genes were performed using both p values and z-scores. The top 20 networks are presented in Fig. 3A, which summarized the networks as an integrated graphical presentation of the molecular mechanisms affected by MWCNT. Notably, a number of the networks identified are critical regulators of immune responses, including RelA (p65 NF-κB subunit), C/EBPbeta, GCR-alpha, PU.1, NRF2, NF-κB, STAT6, and STAT3. Several of the networks play important functions in cell proliferation, cell differentiation, and cell death, including CREB1, SP1, c-Jun, SP3, c-Myc, p53, GCR-alpha, and NF-κB, whereas NRF2 regulates the adaptive response to MWCNT-induced oxidative stress (Dong and Ma 2015b). These findings are consistent with the identified pathways and cellular processes activated by MWCNT discussed above (see Fig. 2B). The STAT6 pathway was shown to be activated by MWCNT, which presumably mediates IL-13 and IL-4-induced signaling and transcription of downstream genes, further supporting activation of a Th2-type response(s) in the lungs by MWCNT (Fig. 3B).

Th2-driven innate immune response to MWCNT exposure in mouse lungs

The identification of prominent IL-13/IL-4 signaling, TSLP signaling, and STAT6 activation by microarray analysis prompted us to further characterize Th2-type response signaling on days 1, 3, 7, and 14 post-exposure to MWCNT.

The Th2 cytokine IL-4 is both an initiator and effector of Th2-type responses critical to the initiation, amplification, and target activation of Th2 effects. Expression of IL-4 in the lungs exposed to MWCNT was examined. The basal expression of IL-4 mRNA in DM-treated lungs was low, but expression was significantly increased on day 1, reached a drastically elevated peak on day 7, and remained significantly elevated through day 14 post-exposure to MWCNT (Fig. 4A). IL-4 protein expression and IL-4-positive cells were barely detectable in DM-treated interstitial lung tissues at all time points examined, as revealed by immunohistochemistry (Fig. 4C, upper images on left and quantification on right). Exposure to MWCNT dramatically increased IL-4 protein expression and the number of IL-4-positive cells, starting from day 1, reaching a significantly higher level on day 3 and a peak on day 7, and lasting at a high level to day 14 post-exposure (Fig. 4C, lower

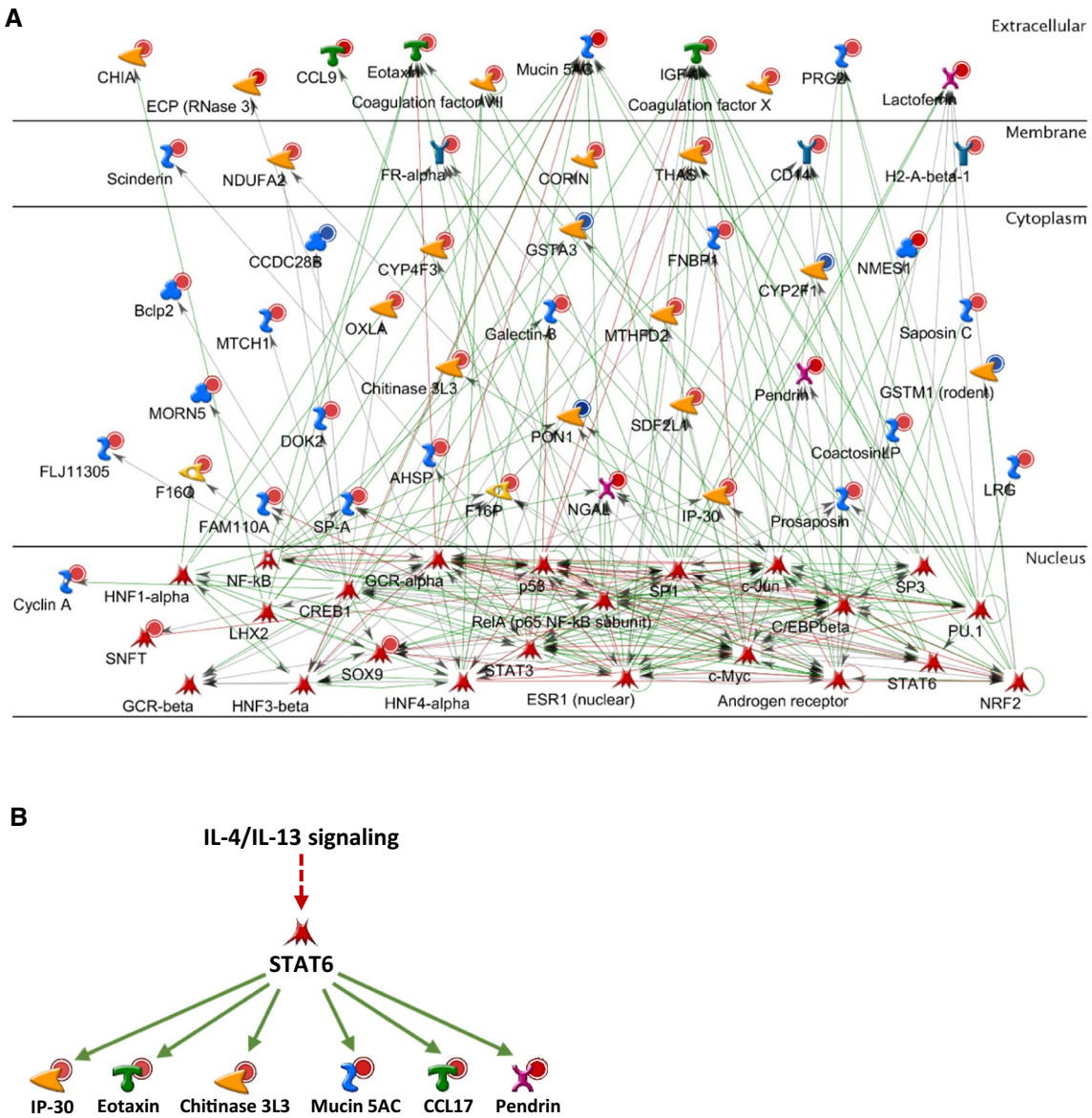

Fig. 3 Upstream regulator and network analysis. **A** The top 20 statistically significant transcriptional regulation networks activated by MWCNT in the lungs were identified and presented. The regulators were presented in the cellular compartments or extracellular space where they play biological functions. Up-regulated molecules with fold changes ≥3 were marked with *dark red dot*, and <3 with *light red dot*; whereas the down-regulated molecules with fold changes ≤−2 were marked with *dark blue dot*, and >−2 with *light blue dot*. The positive/activated relation between two regulators was shown with *green line*, negative/inhibitory relation with *red line*, and unspecified relation with *gray line*. **B** Activation of STAT6 by IL-4 and IL-13 to up-regulate the transcription of a number of target genes in the Th2 response to MWCNT

images on left and quantification on right). A large number of IL-4-positive cells were seen in the peribronchial and perivascular regions in MWCNT-exposed lungs. Induction of IL-4 protein by MWCNT was also confirmed by an ELISA analysis of total lung tissue lysates on day 3 and day 7 post-exposure (data not shown).

IL-13 is another major mediator and effector of Th2 responses. Moreover, IL-13 overlaps with IL-4 in signal transduction and function considerably and plays multiple roles in immune and fibrotic responses. As IL-13 signaling was identified as a major mechanism implicated in the fibrotic response to MWCNT (Fig. 2B), we examined the expression of IL-13 in the lungs. IL-13 mRNA was detected at a low level in DM-treated lungs by qPCR; the expression was significantly induced by MWCNT on day 3, reached a peak on day 7, and was maintained significantly elevated on day 14 post-exposure (Fig. 4B). Expression of IL-13 protein was barely detectable in the interstitial lung tissues

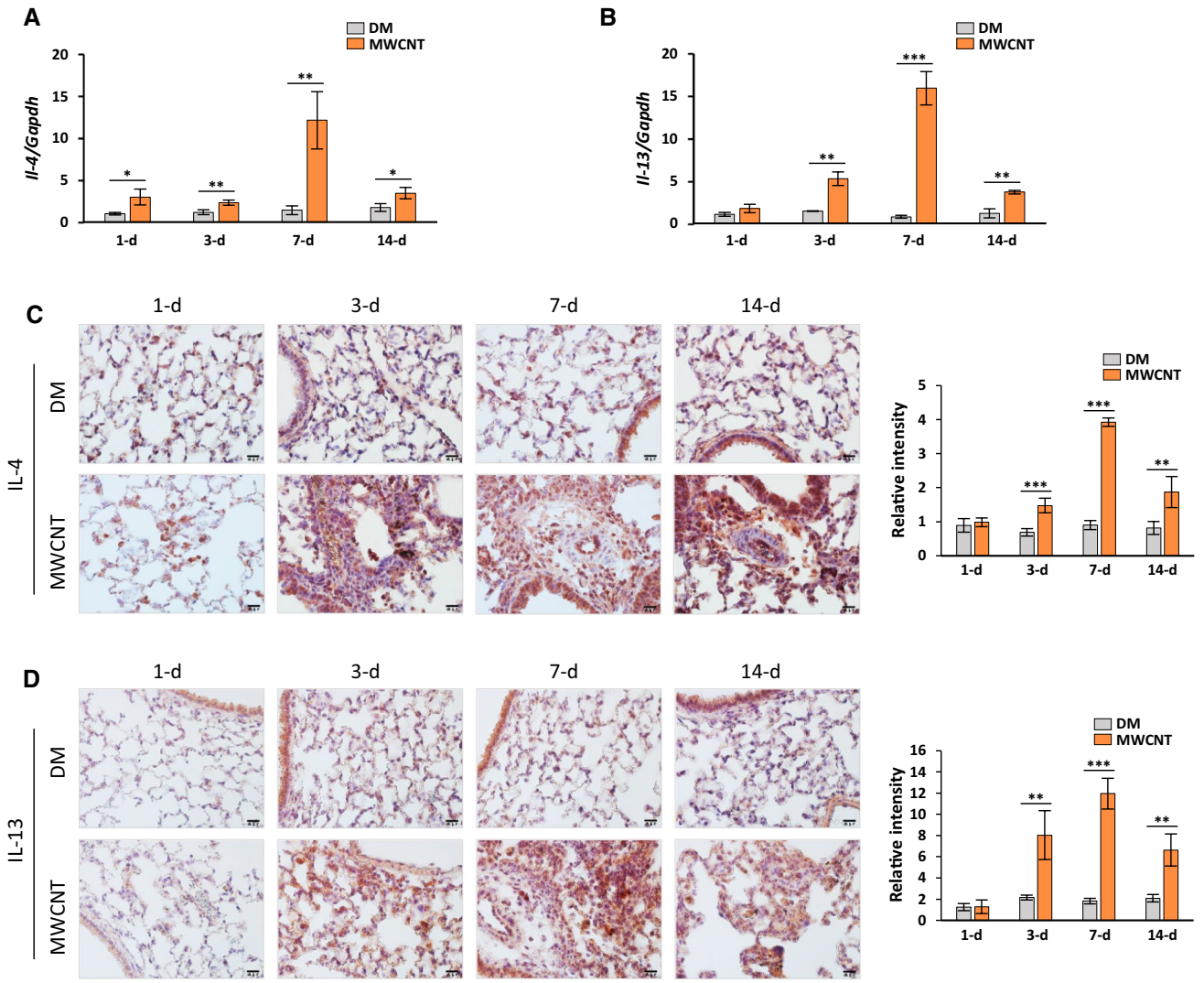

Fig. 4 Induction of IL-4 and IL-13. Total lung RNA was analyzed by qRT-PCR and mRNA levels of IL-4 (**A**) and IL-13 (**B**) relative to that of *Gapdh* were presented as mean ± SD ($n = 3$ for each group). Induction of IL-4 (**C**) and IL-13 (**D**) proteins was observed by immunohistochemistry in the lungs exposed to MWCNT or DM for 1, 3, 7, and 14 days. Shown are images on left and quantification charts (mean ± SD, $n = 4$) on right. *Red* indicates positive staining and *blue* indicates nuclear counterstaining. *Scale bar* 20 μm

exposed to DM at all time points examined by immunohistochemistry staining (Fig. 4D, upper images on left and quantification on right). IL-13 level was markedly elevated, shown as increased numbers of IL-13-positive cells, in lungs treated with MWCNT (Fig. 4D, lower images on left and quantification on right).

Induction of IL-13 mRNA by MWCNT was somewhat delayed compared with that of IL-4: induction was minimal on day 1, became significant on day 3, and lasted through day 14 post-exposure (comparing Fig. 4A, B). ELISA analysis showed that the level of IL-13 in total lung tissue protein lysate was significantly elevated by MWCNT on day 7 and day 14 post-exposure (data not shown), further confirming induction of IL-13 by MWCNT with a slightly delayed time course than IL-4.

A panel of downstream genes regulated by IL-4/IL-13 signaling were induced, including Il4i1 (Interleukin 4 induced 1; Fig. 1), Chia (Chitinase, acidic; AMCase), and Ccl11 (Chemokine (C–C Motif) ligand 11; Eotaxin). The mRNAs of these genes were induced in the lungs by MWCNT at 2.12-fold, 3.65-fold, and 2.15-fold, respectively, as revealed by the microarray analysis (Fig. 2A, Table S1). To validate the induction, we examined the protein expression of these genes in the lungs. Immunohistochemistry analysis revealed that expression of IL4I1, CHIA, or CCL11/Eotaxin protein in DM-treated lungs was barely detectable or low, indicating that Th2-type responses in normal mouse lungs is minimal or undetectable (Fig. 5A, upper images for each protein on left and quantification on right).

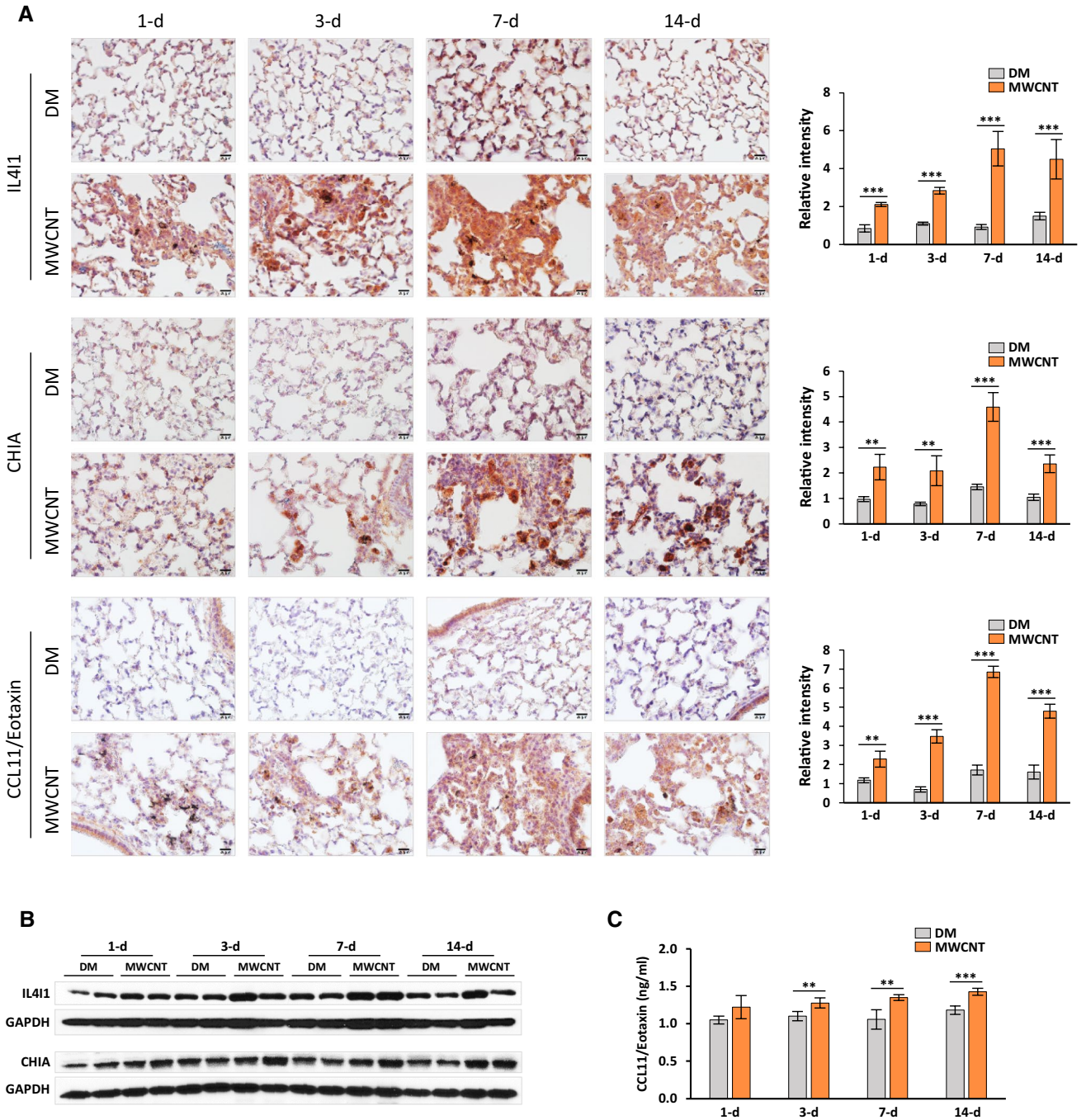

Fig. 5 Induction of Th2 response downstream genes. **A** The protein levels of IL4I1, CHIA and CCL11/Eotaxin were examined on lung sections by immunohistochemistry. Shown are images on *left* and quantification charts (mean ± SD, $n = 4$) on *right*, with *red* for positive staining and *blue* for nuclear counterstaining. *Scale bar* 20 μm. **B** Levels of IL4I1 and CHIA proteins in lung tissues were determined by immunoblotting ($n = 2$ for each group were presented). GAPDH was used as a loading control. **c** Level of CCL11/Eotaxin in lung tissues was detected by ELISA (mean ± SD, $n = 4$)

Expression of IL4I1 was markedly induced in the lungs exposed to MWCNT at all time points examined, with the highest level of IL4I1 occurring on day 7 post-exposure (Fig. 5A, upper panel; images on left and quantification on right). Induced expression of IL4I1 was notably high in areas where MWCNT deposited, which presumably took place in macrophages that engulfed MWCNT. Induction of IL4I1 protein was also observed in total lung tissue lysate by immunoblotting, in particular, on day 7 post-exposure to MWCNT, further demonstrating induction

of this protein in the lungs by MWCNT (Fig. 5B, upper panel).

Expression of CHIA was significantly induced at all time points by MWCNT with a peak on day 7, compared with DM control, as revealed by both immunohistochemistry (Fig. 5A, middle panel; images on left and quantification on right) and immunoblotting (Fig. 5B, lower panel). Interstitial and alveolar macrophages, especially those that engulfed MWCNT, appeared to be a dominant cell type expressing CHIA in MWCNT-treated lungs (Fig. 5A, middle panel).

Expression of CCL11/Eotaxin protein was slightly increased on day 1, but was significantly elevated on days 3, 7, and 14, with the highest expression occurring on day 7, detected by immunohistochemistry. Induction was most apparent in regions of fibrotic foci (Fig. 5A, lower panel; images on left and quantification on right). Elevated expression of CCL11/Eotaxin protein was further confirmed by ELISA analysis of total lung tissue protein lysate from lungs exposed to MWCNT for 3, 7, and 14 days (Fig. 5C).

Taken together, these results clearly demonstrate that these three proteins were up-regulated in the lungs exposed to MWCNT, further confirming activation of a Th2-type response in the lungs by MWCNT.

Th2 cell differentiation and activation in MWCNT-exposed lungs

A hallmark of activation of Th2-type responses is the appearance of Th2 lymphocytes expressing IL-4 and IL-13, albeit other cells, such as basophils and eosinophils, are also important sources of IL-4 during the amplification phase of Th2 responses. We examined whether MWCNT induced

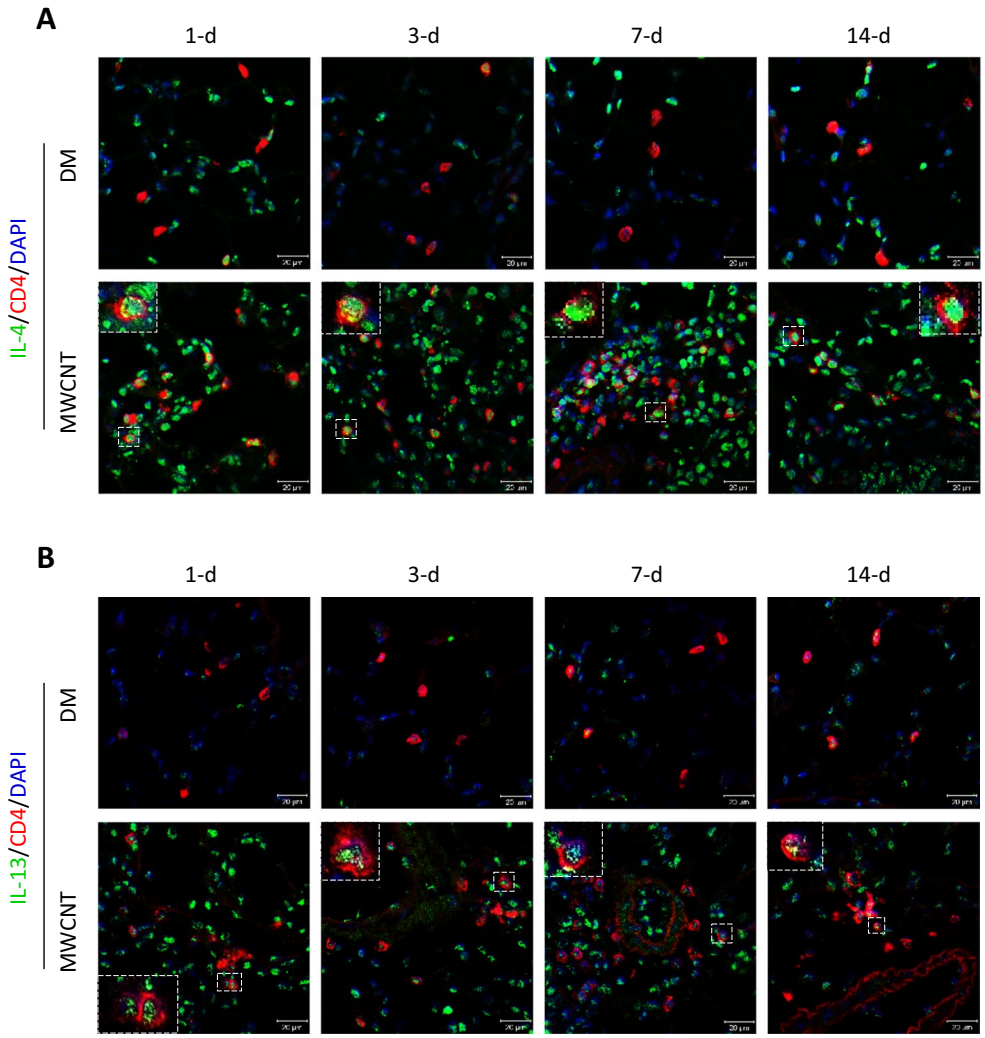

Fig. 6 Detection of Th2-type cytokine expression in lung CD4+ T cells. Expression of IL-4 (**A**) and IL-13 (**B**) in CD4+ T cells was determined by double immunofluorescence staining of the lungs (*scale bar* 20 μm)

expression of IL-4 and IL-13 in CD4+ T cells. Both IL-4-positive cells and CD4+ T cells were detected at low levels in the lungs exposed to DM by double immunofluorescence staining; however, few double-positive cells, i.e., IL-4+ and CD4+ cells, were found (Fig. 6A, upper images). Likewise, IL-13-positive cells and CD4+ T cells were seen at low levels in DM-treated lungs, but few cells were stained positive for both IL-13 and CD4 (Fig. 6B, upper images). These observations indicate that there are few, if any, CD4+ T cells expressing IL-4 or IL-13 in normal lungs.

Exposure to MWCNT markedly increased the numbers of cells expressing IL-4, IL-13, and CD4 in the lungs, respectively (Fig. 6A, B, lower images). Importantly, a significant portion of the cells were stained as double positive for either IL-4 and CD4, or IL-13 and CD4, demonstrating the presence of Th2 cells that express IL-4, or IL-13, or both. It is noteworthy that IL-4- or IL-13-positive cells apparently outnumbered CD4+ cells in MWCNT-treated lungs, indicating that other cells, such as basophils, eosinophils, and macrophages, are potentially activated to express IL-4 and/or IL-13 to amplify Th2 responses. These findings provide direct evidence supporting differentiation of Th2 cells from naïve CD4+ T (Th0) cells and activation of a Th2-type response induced by MWCNT in mouse lungs.

Activation of STAT6 and GATA-3 to mediate Th2-associated gene transcription by MWCNT

Th2-type immune responses depend on the activation of the IL-4Rα/STAT6 pathway, which is elicited by IL-4 through its receptor IL-4R and involves phosphorylation of STAT6 and up-regulation of GATA-3 that transcribes Th2-type cytokines. The p-STAT6 protein (STAT6 phosphorylated at Y641 recognized by a specific monoclonal antibody) and p-STAT6-positive cells were barely detectable or low in number in DM-exposed lungs at all time points examined, but both levels were dramatically increased in the lungs exposed to MWCNT (Fig. 7A, images on left and quantification on right). The increase was particularly apparent in peribronchial and perivascular regions and was persistently high over the entire time period examined, with a peak on day 7 post-exposure. Immunoblotting of total tissue lysate from randomly selected lung samples was performed to verify the activation of STAT6. The total amount of STAT6 protein was not changed by MWCNT, whereas that of p-STAT6 protein was significantly increased by MWCNT, but not DM, at all time points examined (Fig. 7C, upper panel, compare MWCNT with DM). These results clearly showed that MWCNT induced phosphorylation of STAT6.

p-STAT6 forms homodimers in the cytoplasm that translocate into the nucleus to up-regulate expression of GATA-3, which, in turn, up-regulates Th2-type cytokine expression. Whereas GATA-3-positive cells were not detected in the lungs exposed to DM, they were notably increased under exposure to MWCNT, especially in the areas near bronchial and blood vessels, at all time points (Fig. 7B, compare upper and lower images on left; quantification on right). Moreover, the protein level of GATA-3 was markedly increased in the lungs by MWCNT, compared with DM control, as revealed by immunoblotting (Fig. 7C, lower panel, compare MWCNT with DM). Low levels of GATA-3 expression were observed in some but not all mouse lungs exposed to DM, which likely reflects individual variability in the basal expression of GATA-3 protein.

To further validate the activation of Th2 signaling by MWCNT, we examined the lymphocyte specificity of STAT6 and GATA-3 activation. Double immunofluorescence staining revealed that a significantly increased level of p-STAT6 was found in CD4+ T cells (Fig. 8A, upper panel), but not CD45R/B220+ B cells (Fig. 8A, lower panel), in the lungs exposed to MWCNT, compared with DM control. These results indicate that activation of STAT6 by MWCNT occurred in CD4+ T cells, but not B cells, which is consistent with the specific signaling initiated in CD4+ T cells during Th2 responses. Similarly, induction of GATA-3 protein by MWCNT was observed in CD4+ T cells, though expression of GATA-3 was also observed in non-CD4+ cells, which presumably include basophils, eosinophils, and macrophages that were activated to amplify Th2 responses (Fig. 8B). These findings indicate that, under MWCNT exposure, a portion of Th0 cells were stimulated to differentiate into Th2 cells to elicit Th2-type signaling in both Th2 cells and their downstream effector cells in mouse lungs.

Discussion

A prominent feature of CNT-induced lung lesions is the biphasic development of lung fibrosis, wherein CNT elicit a remarkable acute phase inflammatory infiltration and cytokine expression, followed by chronic progression to interstitial fibrosis and granuloma formation (Dong et al. 2015a; Porter et al. 2010). Similar patterns of fibrosis development were observed in other models of induced lung fibrosis including those induced by fibrogenic foreign bodies, which are exemplified by insoluble dusts, such as silica and asbestos, and large biologic masses, such as inhaled allergens and microbes and invading parasites, suggesting a general implication of acute-to-chronic transition in the pathologic development of organ fibrosis. However, little is known about the mechanism(s) controlling the acute-to-chronic transition in induced lung fibrosis.

Acute immune and inflammatory responses are central to elimination of microbes and foreign bodies, but often cause harm to tissues. Fittingly, mammalian species have

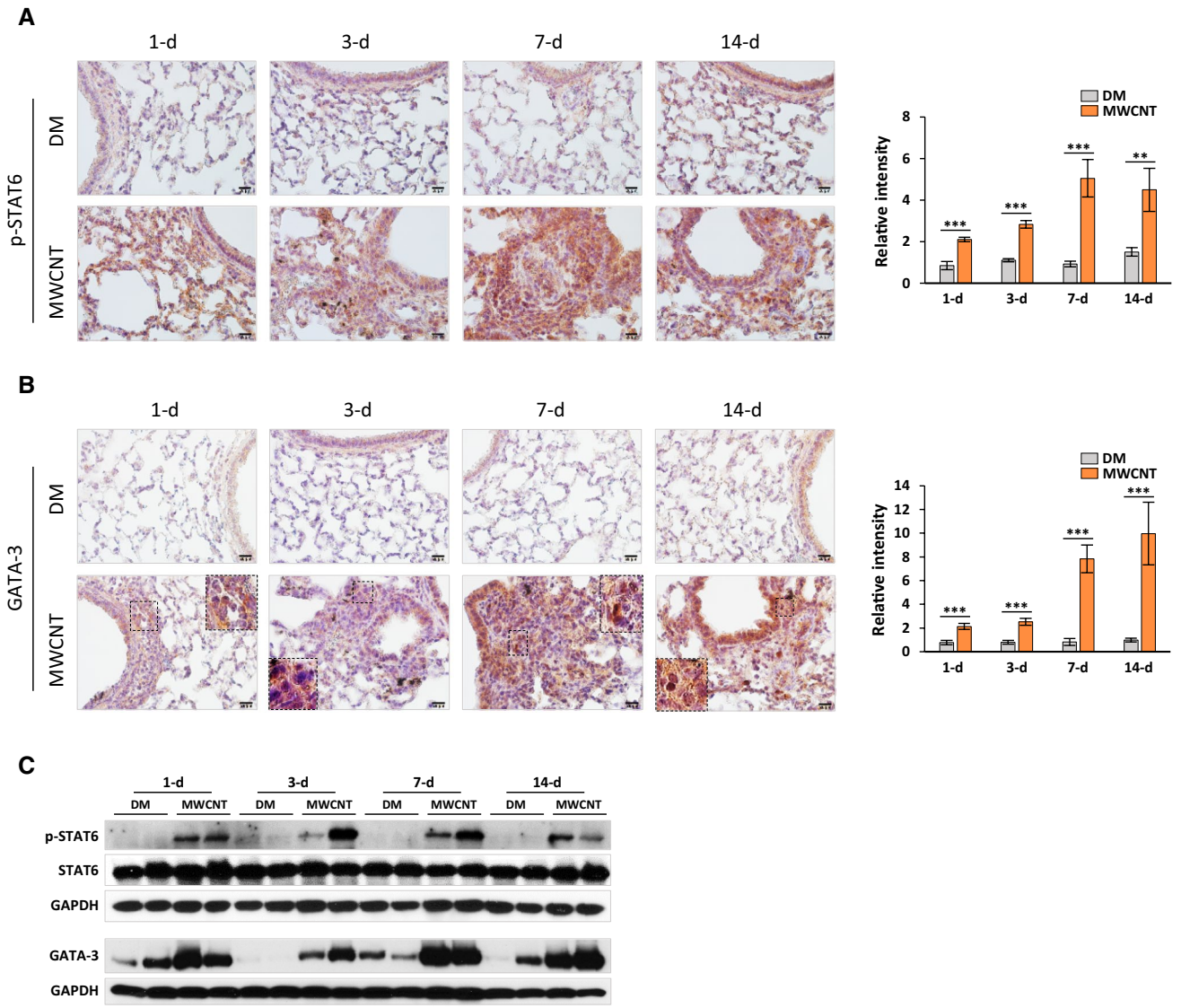

Fig. 7 Activation of STAT6 signaling and up-regulation of GATA-3 expression in mouse lungs. Levels of p-STAT6 (**A**) and GATA-3 (**B**) proteins in the lungs were determined by immunohistochemistry. Shown are images on *left* and quantification charts (mean ± SD, $n = 4$) on *right*, with *red* for positive staining and *blue* for nuclear counterstaining. *Scale bar* 20 μm. **C** Levels of p-STAT6, STAT6, and GATA-3 proteins in lung tissues were detected by immunoblotting ($n = 2$ for each group were presented). GAPDH was used as a loading control

evolved with various strategies to contain acute responses. In the event of an allergen exposure or parasitic infection, Th2-type immune responses would take place to inhibit the T helper 1 (Th1)-driven acute inflammation and, at the same time, promote the containment, destruction, and expulsion of the allergens or worms, and repair damaged tissues (Chen et al. 2012). However, an overzealous or persistent Th2 response would result in progressive and lethal fibrosis (Wynn 2004). By analogy with the findings on this Th1–Th2 interaction, we posit that exposure to CNT in the lungs induces Th2-type responses to abate the tissue-damaging acute inflammation and stimulate the transition to chronic fibrosis, which is in part attributable to CNT's fibrosis-stimulating properties and persistent presence in the lung parenchyma.

Th2-type responses involve complex but defined cellular and molecular events, including the triggering of Th2 cell differentiation from naïve CD4+ T (Th0) cells to IL-4 and IL-13-secreting CD4+ T cells; amplification of the response by recruiting and activating innate immune cells, such as basophils, eosinophils, and macrophages, which further increase Th2-type cytokine production; and effector responses, such as myofibroblast transformation (Wynn 2015). MWCNT have been shown to stimulate allergy-like

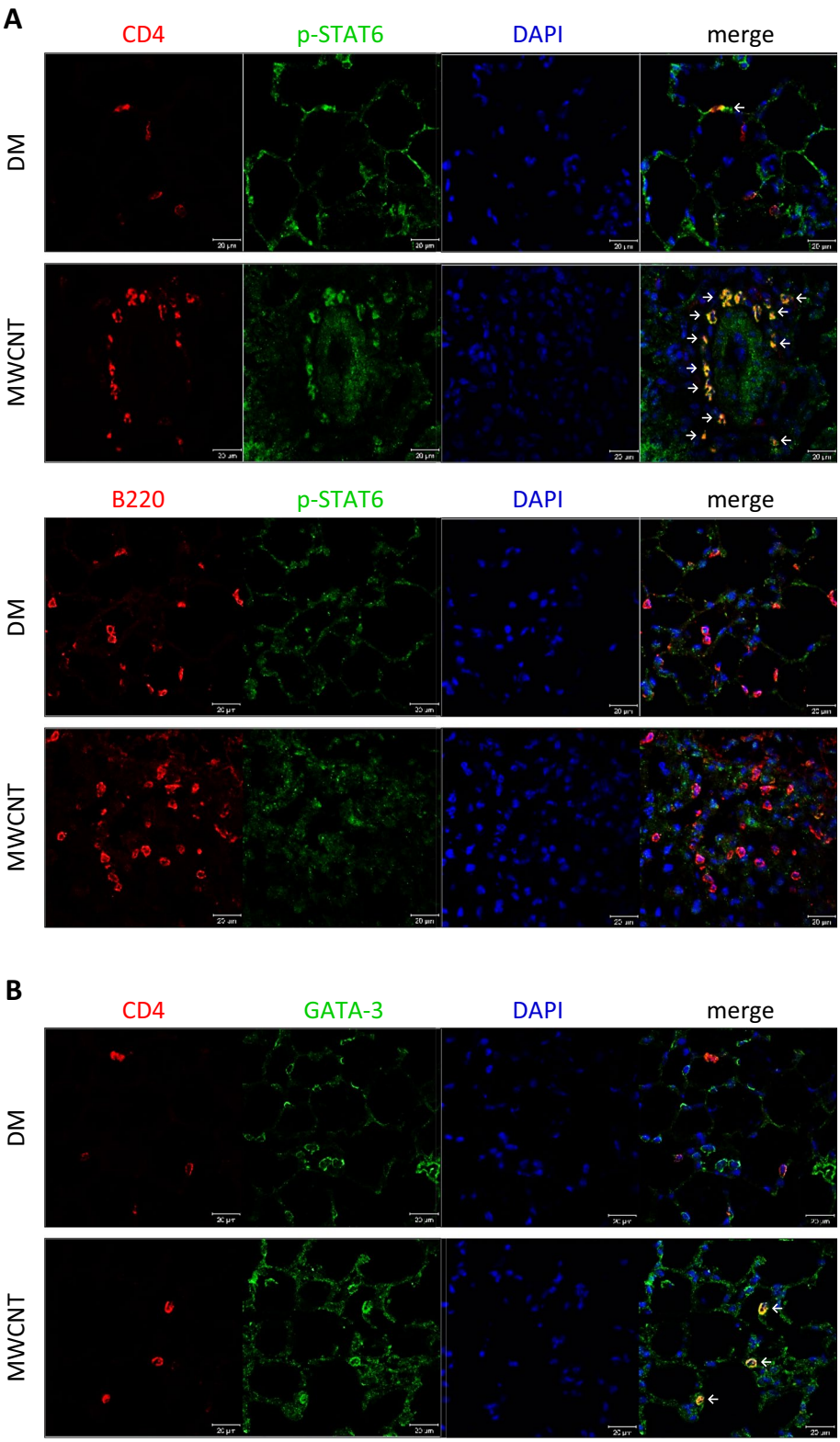

Fig. 8 Lymphocyte activation by MWCNT. Mice were treated with DM or 40 μg MWCNT for 7 days. **A** Phosphorylation of STAT6 was determined in CD4+ T cells (*upper panel*), or in CD45R/B220+ B cells (*lower panel*), by double immunofluorescence staining (*scale bar* 20 μm). **B** Level of GATA-3 expression was detected in CD4+ T cells by double immunofluorescence staining (*scale bar* 20 μm)

inflammation in mouse lung airways where expression of cytokines associated with Th2 functions, i.e., IL-4 and IL-13, was elevated (Rydman et al. 2014). Allergen sensitization was found to induce the expression of IL-4 and IL-13, which appeared to suppress CNT-induced activation of inflammasomes (Shipkowski et al. 2015). The function, cellular origin, and mechanism of induction of the cytokines associated with the allergic responses to CNT

exposure remain to be defined. Evidence demonstrating activation of Th2-driven innate immune responses in CNT-induced lung fibrosis is currently lacking.

In this study, we analyzed the molecular events governing the biphasic pathologic development of lung fibrosis induced by MWCNT. Microarray and computational analyses of the genome-wide gene expression identified differentially expressed genes and affected cellular signaling and biological processes at the junction of acute-to-chronic transition in MWCNT-induced pulmonary fibrotic lesions (Figs. 2, 3; Table S1). Notably, a number of immune/inflammatory responses were persistently identified as major effects triggered by MWCNT. These include a panel of MWCNT-induced differentially expressed genes that play important roles in immune responses, such as Ccl9, Ccl11, Ccl17, Ccl24, Cd14, Dok2, Chi3l3, Chia, Il4i1, Lcn2, Muc5ac, Prg2, and Psap. This finding provides a molecular evidence supporting previous reports that a fibrotic response is preceded and accompanied by an inflammatory response in the lungs exposed to MWCNT (Dong and Ma 2015b; Dong et al. 2015a).

In particular, computational analyses clearly reveal three aspects of Th2-type responses: (a) activation of IL-4 signaling, indicated by up-regulation of Ccl11, Ccl24, Dok2, Il4i1, and Prg2; (b) initiation of IL-13 signaling, indicated by up-regulation of Ccl11, Chi3l3, Chia, Ccl17, and Muc5ac; and (c) activation of transcription factors STAT6 and GATA-3 that mediate transcription of Th2 response target genes. These results indicate that a Th2-type response(s) occur in the lungs at the transition from acute inflammation to chronic lesions during MWCNT-induced lung fibrosis development. In addition, transcription factor analyses reveal that NF-κB, p53 and NRF2 were activated by MWCNT (Fig. 3A). These transcription factors play critical roles in multiple cellular functions and pathways including immune and inflammatory responses, cell growth and differentiation, cell death, and antioxidation. These results are consistent with previous findings regarding the cellular signaling pathways implicated in MWCNT-induced toxicity and pathology (Dong and Ma 2015b; He et al. 2011; Huang et al. 2014; Ravichandran et al. 2010; Takagi et al. 2012).

We performed detailed analyses of Th2-type responses during lung fibrosis under MWCNT exposure on days 1, 3, 7, and 14 after MWCNT administration. First, we showed that MWCNT induced the expression and secretion of Th2-type cytokines IL-4 and IL-13, which are major initiators and effectors of Th2 responses (Fig. 4). Moreover, three downstream molecules in Th2 signaling cascade, i.e., IL4I1, CHIA and CCL11/Eotaxin, whose expression is induced by the activation of IL-4 and/or IL-13 signaling, showed increased levels in the lungs exposed to MWCNT (Fig. 5). We then demonstrated, by double immunofluorescence staining, that increased expression of IL-4 and IL-13 proteins occurred in a sub-population of CD4+ T cells, revealing the differentiation of Th2 cells from naïve CD4+ T cells, a central step in the activation and amplification of Th2 responses (Fig. 6). We further established that the canonical cellular signaling during Th2-type responses, i.e. the IL-4Rα/STAT6 pathway, was activated by MWCNT, starting on day 1 and reaching a peak on day 7 post-exposure to MWCNT, as demonstrated by increased level of phosphorylated STAT6 and enhanced expression of transcription factor GATA-3 responsible for transcriptional up-regulation of Th2-type cytokines (Fig. 7). In addition, we showed that activation of this Th2-type cell signaling took place in CD4+ T cells, but not B220+ B cells, demonstrating the specificity of Th2-associated signaling in lymphocytes (Fig. 8).

IL-4 and IL-13 have been studied intensively in a variety of fibrosing diseases and animal models and have been demonstrated to function as pro-fibrotic mediators to drive fibrosis (Wynn 2004, 2015; Wynn and Ramalingam 2012). IL4I1, CHIA and CCL11/Eotaxin are considered as marker genes of Th2 activation and have been implicated in Th2 mediated functions. These genes were inducible by IL-4 and/or IL-13 in various in vitro and in vivo systems to impact Th2 responses including innate immune functions and organ fibrosis. Our finding that a Th2-type response was significantly induced by MWCNT in the lungs are in agreement with these previous findings.

Taken together, these data provide strong evidence supporting that MWCNT activate a Th2-type response in the lungs, which is promising to play an important role in MWCNT-induced lung fibrosis, as summarized in Fig. 9.

In summary, genome-wide microarray analyses of mouse lungs revealed significant differential gene expression induced by MWCNT at the junction of transition from acute inflammation to chronic fibrosis. Importantly, the analyses uncovered activation of a Th2-type immune/inflammatory response in the lungs, providing a novel mechanism that potentially accounts for exposure-induced lung fibrosis. MWCNT induced expression of IL-4 and IL-13, and a panel of Th2 response associated target genes. Induction of Th2 cytokines took place in Th2 lymphocytes and other Th2 response related cells and required the activation of STAT6 and GATA-3 in Th2 cells that mediate transcription of Th2 effector genes. Our study demonstrates activation of a Th2-driven innate immune response by MWCNT in the lungs, providing a

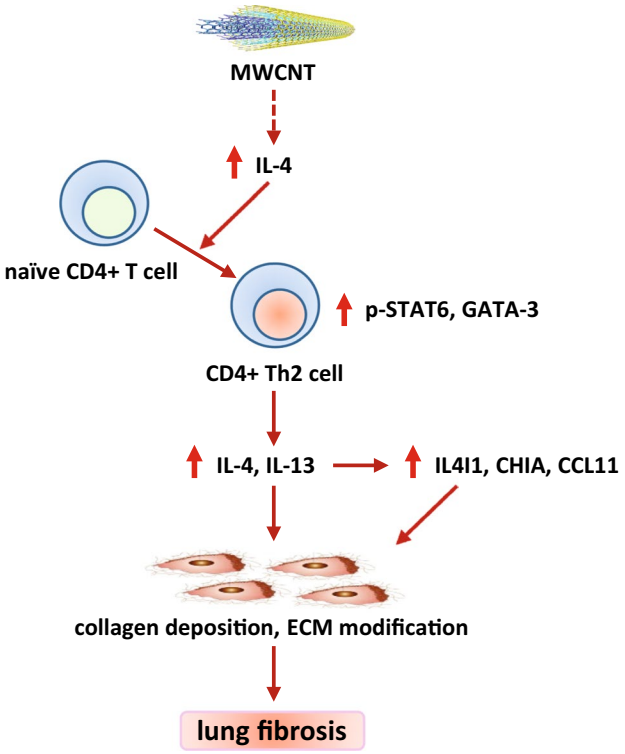

Fig. 9 Schematic presentation of induction of a Th2-driven innate immune response in MWCNT-induced lung fibrosis

novel, testable model in which the interplay between Th2-driven innate immune functions and lung fibrosis induced by MWCNT can be analyzed at molecular and cellular levels in vivo.

Acknowledgments This work was funded to QM by National Institute for Occupational Safety and Health, Health Effects Laboratory Division and Nanotechnology Research Center.

Compliance with ethical standards

Conflict of interest The authors declare that they have no conflict of interest.

Ethical approval All applicable international, national, and/or institutional guidelines for the care and use of animals were followed. All procedures performed in studies involving animals were in accordance with the ethical standards of the institution or practice at which the studies were conducted.

References

Aiso S, Yamazaki K, Umeda Y et al (2010) Pulmonary toxicity of intratracheally instilled multiwall carbon nanotubes in male fischer 344 rats. Ind Health 48(6):783–795

Chen F, Liu Z, Wu W et al (2012) An essential role for TH2-type responses in limiting acute tissue damage during experimental helminth infection. Nat Med 18(2):260–266. doi:10.1038/nm.2628

De Volder MF, Tawfick SH, Baughman RH, Hart AJ (2013) Carbon nanotubes: present and future commercial applications. Science 339(6119):535–539. doi:10.1126/science.1222453

Donaldson K, Murphy FA, Duffin R, Poland CA (2010) Asbestos, carbon nanotubes and the pleural mesothelium: a review of the hypothesis regarding the role of long fibre retention in the parietal pleura, inflammation and mesothelioma. Part Fibre Toxicol 7:5. doi:10.1186/1743-8977-7-5

Dong J, Ma Q (2015a) Advances in mechanisms and signaling pathways of carbon nanotube toxicity. Nanotoxicology 9:658–676. doi:10.3109/17435390.2015.1009187

Dong J, Ma Q (2015b) Suppression of basal and carbon nanotube-induced oxidative stress, inflammation and fibrosis in mouse lungs by Nrf2. Nanotoxicology. doi:10.3109/17435390.2015.1110758

Dong J, Porter DW, Batteli LA, Wolfarth MG, Richardson DL, Ma Q (2015a) Pathologic and molecular profiling of rapid-onset fibrosis and inflammation induced by multi-walled carbon nanotubes. Arch Toxicol 89(4):621–633. doi:10.1007/s00204-014-1428-y

Dong J, Yu X, Porter DW, Battelli LA, Kashon ML, Ma Q (2015b) Common and distinct mechanisms of induced pulmonary fibrosis by particulate and soluble chemical fibrogenic agents. Arch Toxicol 90(2):385–402. doi:10.1007/s00204-015-1589-3

Duffield JS, Lupher M, Thannickal VJ, Wynn TA (2013) Host responses in tissue repair and fibrosis. Ann Rev Pathol 8:241–276. doi:10.1146/annurev-pathol-020712-163930

Han YG, Xu J, Li ZG, Ren GG, Yang Z (2012) In vitro toxicity of multi-walled carbon nanotubes in C6 rat glioma cells. Neurotoxicology 33(5):1128–1134. doi:10.1016/j.neuro.2012.06.004

He X, Young SH, Schwegler-Berry D, Chisholm WP, Fernback JE, Ma Q (2011) Multiwalled carbon nanotubes induce a fibrogenic response by stimulating reactive oxygen species production, activating NF-kappaB signaling, and promoting fibroblast-to-myofibroblast transformation. Chem Res Toxicol 24(12):2237–2248. doi:10.1021/tx200351d

Huang X, Zhang F, Sun X et al (2014) The genotype-dependent influence of functionalized multiwalled carbon nanotubes on fetal development. Biomaterials 35(2):856–865

Husain AN, Kumar V (2005) The lung. In: Kumar V, Abbas AK, Fausto N (eds) Robbins and cotran pathologic basis of disease, 7th edn. Elsevier Saunders, Philadelphia, pp 711–772

Johnston HJ, Hutchison GR, Christensen FM et al (2010) A critical review of the biological mechanisms underlying the in vivo and in vitro toxicity of carbon nanotubes: the contribution of physico-chemical characteristics. Nanotoxicology 4(2):207–246. doi:10.3109/17435390903569639

Lam CW, James JT, McCluskey R, Hunter RL (2004) Pulmonary toxicity of single-wall carbon nanotubes in mice 7 and 90 days after intratracheal instillation. Toxicol Sci 77(1):126–134. doi:10.1093/toxsci/kfg243

Ma-Hock L, Strauss V, Treumann S et al (2013) Comparative inhalation toxicity of multi-wall carbon nanotubes, graphene, graphite nanoplatelets and low surface carbon black. Part Fibre Toxicol 10:23. doi:10.1186/1743-8977-10-23

Morgan WKC, Seaton A (1995) Occupational lung diseases, 3rd edn. W.B. Saunders Company, Philadelphia

Porter DW, Hubbs AF, Mercer RR et al (2010) Mouse pulmonary dose- and time course-responses induced by exposure to multi-walled carbon nanotubes. Toxicology 269(2–3):136–147. doi:10.1016/j.tox.2009.10.017

Ravichandran P, Baluchamy S, Sadanandan B et al (2010) Multi-walled carbon nanotubes activate NF-kappaB and AP-1 signaling pathways to induce apoptosis in rat lung epithelial cells. Apoptosis Int J Program Cell Death 15(12):1507–1516. doi:10.1007/s10495-010-0532-6

Reddy AR, Reddy YN, Krishna DR, Himabindu V (2012) Pulmonary toxicity assessment of multiwalled carbon nanotubes in rats

following intratracheal instillation. Environ Toxicol 27(4):211–219. doi:10.1002/tox.20632

Rydman EM, Ilves M, Koivisto AJ et al (2014) Inhalation of rod-like carbon nanotubes causes unconventional allergic airway inflammation. Part Fibre Toxicol 11:48. doi:10.1186/s12989-014-0048-2

Shipkowski KA, Taylor AJ, Thompson EA et al (2015) An allergic lung microenvironment suppresses carbon nanotube-induced inflammasome activation via STAT6-dependent inhibition of caspase-1. PLoS ONE 10(6):e0128888. doi:10.1371/journal.pone.0128888

Shvedova AA, Kisin ER, Mercer R et al (2005) Unusual inflammatory and fibrogenic pulmonary responses to single-walled carbon nanotubes in mice. Am J Physiol Lung Cell Mol Physiol 289(5):L698–L708. doi:10.1152/ajplung.00084.2005

Siegrist KJ, Reynolds SH, Kashon ML et al (2014) Genotoxicity of multi-walled carbon nanotubes at occupationally relevant doses. Part Fibre Toxicol 11:6. doi:10.1186/1743-8977-11-6

Takagi A, Hirose A, Futakuchi M, Tsuda H, Kanno J (2012) Dose-dependent mesothelioma induction by intraperitoneal administration of multi-wall carbon nanotubes in p53 heterozygous mice. Cancer Sci 103(8):1440–1444. doi:10.1111/j.1349-7006.2012.02318.x

Wang P, Nie X, Wang Y et al (2013) Multiwall carbon nanotubes mediate macrophage activation and promote pulmonary fibrosis through TGF-beta/Smad signaling pathway. Small 9(22):3799–3811. doi:10.1002/smll.201300607

Wynn TA (2004) Fibrotic disease and the T(H)1/T(H)2 paradigm. Nat Rev Immunol 4(8):583–594. doi:10.1038/nri1412

Wynn TA (2015) Type 2 cytokines: mechanisms and therapeutic strategies. Nat Rev Immunol 15(5):271–282. doi:10.1038/nri3831

Wynn TA, Ramalingam TR (2012) Mechanisms of fibrosis: therapeutic translation for fibrotic disease. Nat Med 18(7):1028–1040. doi:10.1038/nm.2807

Zhang Q, Huang JQ, Qian WZ, Zhang YY, Wei F (2013) The road for nanomaterials industry: a review of carbon nanotube production, post-treatment, and bulk applications for composites and energy storage. Small 9(8):1237–1265. doi:10.1002/smll.201203252